

Stability of RVB hole stripes in high-temperature superconductors

Manuela Capello,¹ Marcin Raczkowski,² Didier Poilblanc¹

¹ *Laboratoire de Physique Théorique UMR 5152,*

CNRS and Université Paul Sabatier, F-31062 Toulouse, France

² *Marian Smoluchowski Institute of Physics, Jagellonian University, Reymonta 4, PL-30059 Kraków, Poland*

(Dated: October 31, 2018)

Indications of density-wave states in underdoped cuprates, coming from recent STM (scanning tunneling microscopy) and Hall-resistance measurements, have raised new concerns whether stripes could be stabilized in the superconducting phase of cuprate materials, even in the absence of antiferromagnetism. Here, we investigate this issue using state-of-the-art quantum Monte Carlo calculations of a $t - J$ model. In particular we consider the stability of unidirectional hole domains in a modulated superconducting background, by taking into account the effect of tetragonal-lattice distortions, next-nearest neighbor hopping and long-range Coulomb repulsion.

I. INTRODUCTION

The physics of high-temperature superconductors (HTSC) is characterized by the presence of several competing orders. Besides antiferromagnetism and superconductivity, it is now widely accepted that the underdoped region of the HTSC phase diagram shows a pseudogap phase^{1,2} and occasionally the presence of spatially-ordered states^{3,4} at special dopings, characterized by charge domain walls separated by antiferromagnetic regions. Recently, accurate STM experiments⁵ have revealed modulations of the local density of states in the form of unidirectional domains for two different underdoped HTSC materials, $\text{Ca}_{2-\delta}\text{Na}_\delta\text{CuO}_2\text{Cl}_2$ and $\text{Bi}_2\text{Sr}_2\text{CaCu}_2\text{O}_{8+\delta}$, where spatial ordering was not detected before. These findings highlight the importance of inhomogeneous states as a general feature of HTSC, and extend the idea of quasi-one dimensional order beyond the original spin-stripe picture⁶, with superconductivity coexisting with charge modulation, in the absence of antiferromagnetism. Moreover, recent measurements of Hall resistance⁷ on underdoped $\text{YBa}_2\text{Cu}_3\text{O}_\delta$ and $\text{YBa}_2\text{Cu}_4\text{O}_8$ give evidence of a reconstruction of the Fermi surface caused by the onset of a density-wave phase in the large-field induced normal state, indicating that spatial symmetry breaking is a common characteristic of underdoped cuprates.

Theoretically, it is challenging to characterize a modulated state that could mimic the experimental findings, and to identify the key microscopic parameters that could induce this kind of non-uniform superconducting phases. Indeed, besides the strong, local repulsion among electrons, that leads to antiferromagnetism, the low-energy physics of cuprates is often determined by additional hopping integrals among next-nearest neighbor copper atoms, and by a long-range Coulomb repulsion among electrons. These terms have been studied in the past for different inhomogeneous states and were found to stabilize modulated superstructures^{8,9}. Also of relevance, is the role played by structural instabilities, a feature undoubtedly present in many HTSC compounds, in stabilizing modulated superstructures. Indeed, HTSC are often characterized by a low-temperature tetragonal phase¹⁰,

produced by a tilt of the oxygen octahedra that leads to a different electronic hopping and exchange integral along the two planar directions. Previous calculations found that spatial anisotropy could stabilize antiferromagnetic-stripe phases^{11,12}. Therefore, in view of what is found in experiments, it is important to understand if a similar effect occurs for *superconducting* modulated states.

In this paper, we study the competition among homogeneous and non-uniform superconducting states, by taking into account the presence of spatial lattice distortions, next-nearest neighbors hopping terms and long-range Coulomb repulsion. As a prototype model for cuprate superconductors, we investigate the $t - J$ model¹³ in two dimensions, by using state-of-the-art Variational Monte Carlo techniques (supplemented by mean-field approaches). Following Anderson idea¹⁴, the variational approach, based on the resonating-valence-bond (RVB) wavefunction, has successfully described most of the features of HTSC^{15,16}. However, to tackle spatially-inhomogeneous superconducting states like those found by experiments, more involved calculations, including the possibility of local modulations in the superconducting state, are required. Here, we accomplish this task and show that, generically, half-filled hole stripes can form easily in a RVB superconductor at quite small energy cost. Interestingly enough, lattice distortion and long-range Coulomb repulsion are proved to play a key role.

This paper is organized as follows. In Section II we introduce the model and the variational approach, presenting the two families of modulated wavefunctions that we study, the π -phase shift and inphase domain RVB wavefunctions. In Section III we characterize in detail the new inphase domain RVB state, introduced in this paper, for the $t - J$ model. In Section IV, V and VI we show the effect of lattice distortion, next-nearest neighbor hopping and long-range Coulomb repulsion, respectively, on the stabilization of modulated superconducting states. Finally, in Section VII we draw our conclusions.

II. MODEL AND WAVEFUNCTIONS

The $t - J$ Hamiltonian is defined, using standard notations, as¹³:

$$H_{t-J} = -t \sum_{\langle i,j \rangle \sigma} \alpha_{ij} (\tilde{c}_{i\sigma}^\dagger \tilde{c}_{j\sigma} + h.c.) + J \sum_{\langle i,j \rangle} \alpha_{ij}^2 \mathbf{S}_i \cdot \mathbf{S}_j \quad (1)$$

where $\tilde{c}_{i\sigma}^\dagger = (1 - n_{i-\sigma})c_{i\sigma}^\dagger$ acts on the reduced Hilbert space with no double occupancies. For non-distorted lattices we take $\alpha_{ij} = \alpha_x = \alpha_y = 1$ for all nearest neighbors. Instead, tetragonal distortion is set by taking different hopping and exchange parameters along the x and y direction, according to the position of the tilt axis. This implies $\alpha_x \neq \alpha_y$, with $\alpha_x < 1$ ($\alpha_y < 1$) and $\alpha_y = 1$ ($\alpha_x = 1$) respectively for the tilt axis along the y (x) direction. Here, we mainly focus on the physically relevant case $t/J = 3$ (if not specified otherwise) at doping $\delta = 1/8$.

In the following, we make use of the Variational Monte Carlo techniques (VMC), using clusters of $N = 8 \times 8$, 128 (45 degree $8^2 + 8^2$ tilted lattice) and 16×16 sites with periodic-boundary conditions. Moreover, to have access to larger sizes that can approach the thermodynamic limit, we compare our variational results with predictions coming from the renormalized mean-field theory (RMFT)¹⁷, on a 128×128 cluster, using unit cell translation symmetry¹⁸ (for more details on the RMFT results, see Ref.¹⁹). In the variational procedure, the RVB state is derived from the BCS mean-field state by incorporating the effect of correlation via the so-called Gutzwiller projector \mathcal{P}_g , that can be treated exactly within the quantum Monte Carlo scheme. Indeed, given the mean-field Hamiltonian:

$$H_{MF} = \sum_{i,j\sigma} (\chi_{ij} c_{i\sigma}^\dagger c_{j\sigma} + h.c.) + \sum_{\langle i,j \rangle} (\Delta_{ij} c_{i\uparrow}^\dagger c_{j\downarrow}^\dagger + h.c.) + \mu \sum_{i\sigma} n_{i\sigma} \quad (2)$$

we construct the variational state by applying the Gutzwiller projector to the ground state $|D\rangle$ of Eq. (2):

$$|\Psi_G\rangle = \mathcal{P}_g |D\rangle = \prod_i (1 - n_{i\uparrow} n_{i\downarrow}) |D\rangle \quad (3)$$

where $n_{i\sigma}$ counts the number of electrons of spin σ on site i . The terms χ_{ij} , Δ_{ij} and μ in Eq. (2) correspond to a set of parameters that are optimized in order to minimize the variational energy, according to the stochastic minimization algorithm²⁰. In the simple case of the uniform RVB state, the independent parameters reduce to μ and $\Delta_{ij} = \pm\Delta$ for nearest neighbors, with the sign following the d -wave symmetry. Moreover, another competing homogeneous state, the staggered-flux phase²¹ (SFP), is obtained by allowing the hopping parameters χ_{ij} to be complex, leading to staggered currents circulating in opposite directions in the neighboring plaquettes.

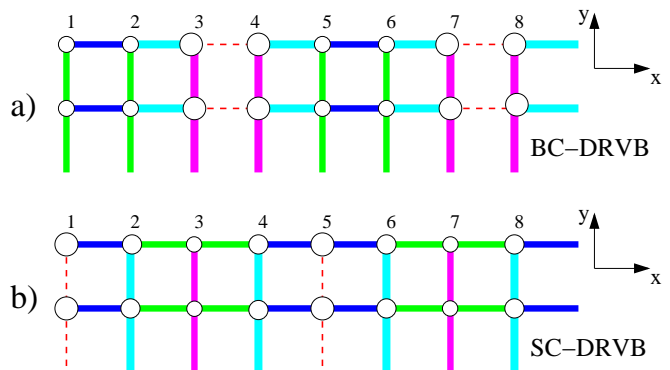


FIG. 1: (Color online) Cartoon of the (a) bond-centered and (b) site-centered domain RVB (DRVB) stripes. Non-equivalent bonds have different colors. Thicker (larger) bonds (circles) have larger pairing (hole) densities. Dashed lines indicate bonds where Δ_{ij} is set to zero.

Here, we study possible instabilities of the RVB state towards spatial modulations, allowing the RVB bonds Δ_{ij} to become inhomogeneous. In particular, it is known from experiments that one-dimensional hole-rich regions are generally spaced by $1/(2\delta)$, implying half-filled hole domains with an average of one hole every $1/\delta$ sites in the direction where translational symmetry is broken. At a doping of $\delta = 1/8$, this corresponds to a periodicity of four lattice spacings $4a$. Remarkably, we found such states, where hole-rich stripes coexist with modulated superconducting domains, whose energy per site is only of a very small fraction of J higher than its uniform counterpart. The hierarchy of phases is therefore expected to be very sensitive to the details of the microscopic Hamiltonian.

In a previous paper²², we considered a variational domain-RVB state that contains a π -phase shift in the superconducting order parameter between regions of four-lattice spacings width (π DRVB). The phase shifts create domain walls with vanishing pairing amplitude and a consequent concentration of holes. The π DRVB states turned out to be competitive with respect to the homogeneous RVB state, and could explain the copper-oxygen layer decoupling found in $\text{La}_{2-x}\text{Ba}_x\text{CuO}_4$, accompanied by a depression of T_c at $1/8$ doping^{23,24}. Here, we complete the characterization of π DRVB states, by considering the effect of lattice distortion, nearest-neighbor hopping term, and long-range Coulomb repulsion. Moreover, since the presence of the antiphase domains implies a certain amount of energy, in the following we investigate an alternative strategy to tackle the problem, and propose another possible candidate for superconducting stripes, where domains are inphase: the domain RVB state (DRVB). Starting from the RVB state, we investigate the energy cost associated to the introduction of line defects in the uniform state, in the form of unidirectional hole domains. This is done by imposing a vanishing pairing amplitude $\Delta_{ij} = 0$ along one direction, with

TABLE I: VMC and RMFT energy per site (in units of t) for different projected wavefunctions for the $t - J$ model at doping $1/8$.

$ D\rangle$	$E_{VMC} [t]$	$E_{RMFT} [t]$
RVB	-0.45564(3)	-0.4549(1)
SFP	-0.44630(3)	-0.4286(1)
π DRVB [Ref. ²²]	-0.44529(3)	-0.4413(1)
BC-DRVB	-0.45490(3)	-0.4511(1)
SC-DRVB	-0.45525(3)	-0.4507(1)

a periodicity that, at doping $1/8$, corresponds to $4a$. In Figure 1 we show the two possible modulations of the inphase DRVB state derived from the above arguments. In Figure 1(a) stripes are bond-centered (BC), with the RVB bonds characterized by a periodicity of $4a$ along the x direction. The pairing field Δ_{ij} associated to one type of horizontal bonds is set to zero. Alternatively, in Figure 1(b) the stripes are site-centered (SC), where the lines of vertical bonds with $\Delta_{ij} = 0$ are separated by $4a$ along the x direction.

Besides the π -shift domain RVB stripes, which could give a natural explanation to the decoupling among superconducting layers, this second class of superconducting hole stripes, the DRVB states, could be related to the STM experimental findings of inhomogeneous superconducting states.

III. DRVB STRIPES IN THE $t - J$ MODEL

In this section we characterize the new inphase domain RVB states for the $t - J$ model, showing that, among the superconducting stripe states^{22,25}, they constitute a valid candidate for a strongly-competing, inhomogeneous state. We start by considering the variational energies of the different stripe states, together with the corresponding RMFT values in Table I. Both approaches show that, with respect to the SFP and the π DRVB²² states, the DRVB states are one order of magnitude closer in energy to the homogeneous RVB phase. Note that the site-centered variational energy approaches the RVB state very closely. However, in both cases the small energy difference indicates both DRVB states as very promising candidates for a competing inhomogeneous state. Remarkably, within the DRVB geometry, the suppression of some of the RVB bonds does not imply significant energy costs. Notice that, at the variational level, the optimal wavefunctions preserve the d -wave symmetry of the pairing field in the regions where $\Delta_{ij} \neq 0$, with a small modulation that depends upon the type of bond (see Figure 1).

To prove that the non-homogeneous DRVB wavefunctions that we have constructed indeed correspond to spatially modulated states, we show in Figure 2 typical profiles in the bond- and site-centered states. It turns out that the hole distribution along the different sites of the

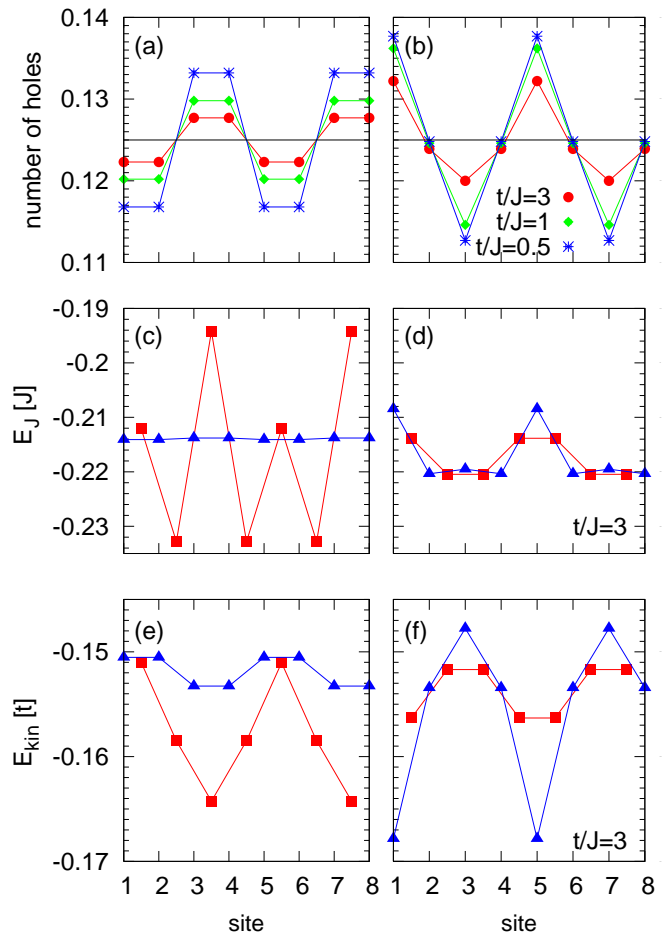


FIG. 2: (Color online) Top panel: Hole distribution in DRVB states for different values of t/J as shown in graph. Middle and bottom panel: Magnetic (in units of J) and kinetic (in units of t) bond energy within the unitary cell of Figure 1 for $t/J = 3$. Squares indicate energies associated to horizontal bonds (located between two sites), triangles to vertical bonds. Left panels refer to the BC-DRVB state and right panels to the SC-DRVB state. All quantities are calculated for a cluster of 16×16 sites.

unitary cell is non-uniform, the hole density being larger along the regions where $\Delta_{ij} = 0$ (notice that the magnitude of the hole modulation increases with J/t). Moreover, the magnetic and kinetic energies follow the same modulation than the charge. Indeed, along the $\Delta_{ij} = 0$ bonds the kinetic energy is enhanced, while the magnetic energy is suppressed, as expected. Note that the bonds presenting the largest modulation are the horizontal (vertical) ones for the BC (SC) wavefunction, i.e., the bonds along the direction where some of the pairing fields are suppressed.

Finally, to characterize the superconducting properties of our variational states, we calculate the singlet pairing

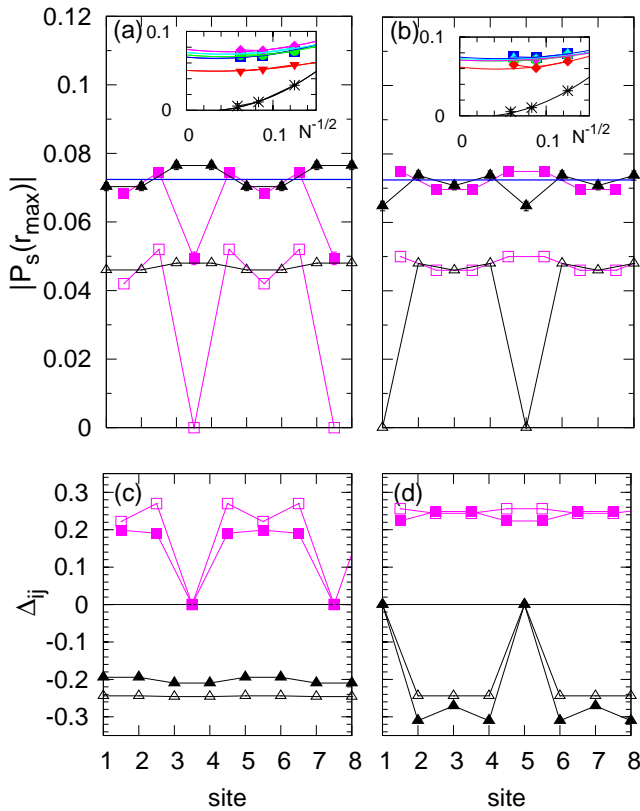


FIG. 3: (Color online) Top panel: Pairing order parameter (filled points for VMC, empty points for RMFT) for the BC-DRVB (left) and SC-DRVB (right) states along the 8 independent sites of Figure 1. Squares correspond to horizontal bonds (located between two sites), triangles to vertical bonds. The blue line corresponds to the pairing order parameter in the homogeneous RVB state. Inset: size scaling of the pairing order parameter as a function of the inverse-squared number of sites. Colors refer to the corresponding colored bonds of Figure 1. Stars correspond to the projected Fermi sea, for comparison. Bottom panel: corresponding pairing variational parameters for the different bonds.

correlations:

$$P_s^2(r) = \frac{\langle \Psi_G | \tilde{\Delta}_{s+r}^\dagger \tilde{\Delta}_s | \Psi_G \rangle}{\langle \Psi_G | \Psi_G \rangle}, \quad (4)$$

where $\tilde{\Delta}_s^\dagger = c_{s,\uparrow}^\dagger c_{s+\hat{a},\downarrow}^\dagger - c_{s,\downarrow}^\dagger c_{s+\hat{a},\uparrow}^\dagger$ creates a singlet pair of electrons among nearest neighbors for each independent site s of the unitary cell in Figure 1 and \hat{a} is the unit vector, that specifies the bond direction (along x or y). We extract the pairing order parameter by taking the square root $P_s(r_{max})$ of the pairing correlation function (4) at the maximum distance r_{max} for different cluster sizes, for all independent sites. Notice that the VMC and RMFT profiles are in agreement. However, within VMC, we find, for all different bonds, that the pairing order parameter is finite, see Figure 3. Remarkably, this is the case also for the bond where the variational parameter $\Delta_{ij} = 0$, signaling that the Gutzwiller approximation

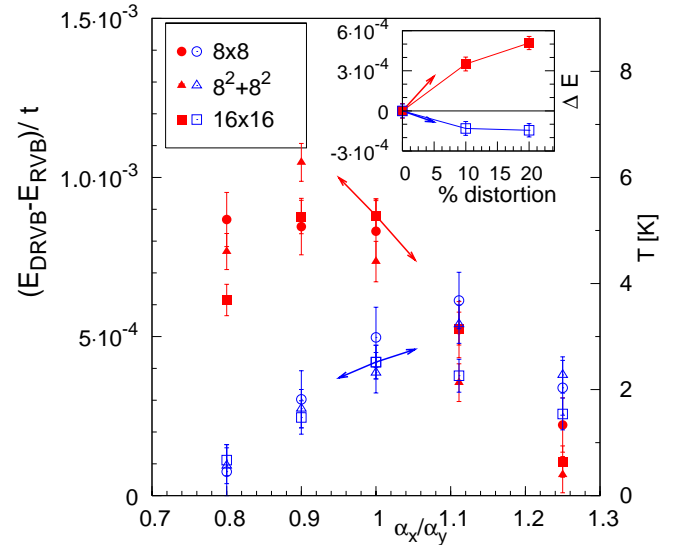


FIG. 4: (Color online) Energy difference between the BC-DRVB (SC-DRVB) and the homogeneous RVB state²⁷ as a function of the lattice distortion α_x/α_y , shown by filled (empty) symbols. Charge stripes are arranged along the y direction in all cases. Energies (per site) are reported in units of t , for the case $t/J = 3$. The right axis is a temperature scale, assuming $J = 2000K$. The points considered correspond to distortions of 10% and 20% in the two directions. Inset: Energy difference among the two possible stripe arrangements, parallel and perpendicular to the tilt axis, for BC and SC wavefunctions. Arrows correspond to the predictions given by the Hellman-Feynman theorem for the largest system.

is not accurate in this case. The resulting picture consists of two different types of bonds, some associated to the hole-rich region, and others where the superconducting order parameter, although slightly enhanced or depressed locally, is very close the one found for the homogeneous RVB state. This feature, together with the non-uniform charge distribution, has strong similarities with the picture which could be derived from the STM experimental findings of Ref.⁵.

IV. LATTICE DISTORTION

Considering the $t - J$ Hamiltonian of Eq. (1), lattice distortion is set by imposing two different α_{ij} along the x and y direction. We find that setting $\alpha_x \neq \alpha_y$ further increases the stabilization of the non-homogeneous states. This feature, that was already observed in the context of spin-stripes^{11,12}, extends its validity in the quite different case of superconducting-stripe states. Considering the case of DRVB states, we find that the bond-centered stripes gain a remarkable amount of energy upon distortion, see Figure 4. In particular, we find that the superconducting inphase domain stripes are stabilized²⁶ when the $\Delta_{ij} = 0$ bonds lie along the direction of the

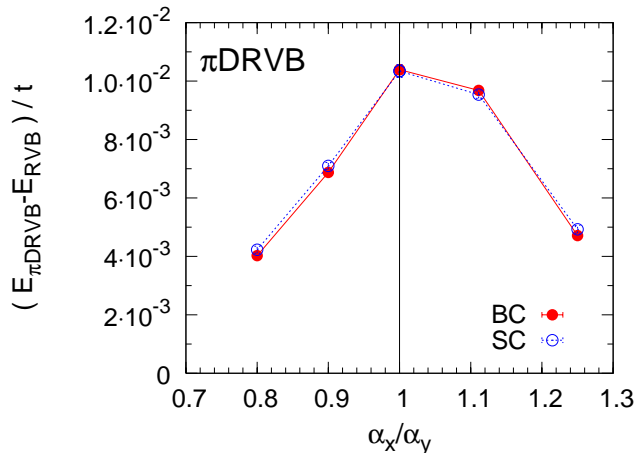


FIG. 5: (Color online) Energy difference between the BC- π DRVB (SC- π DRVB) and the homogeneous RVB state²⁷ as a function of the lattice distortion α_x/α_y , shown by filled (empty) symbols. Charge stripes are arranged along the y direction in all cases. Energies (per site) are reported in units of t . The points considered correspond to distortions of 10% and 20% in the two directions.

tilt axis, where the hopping and exchange parameters are the largest. Assuming by convention the hole-stripe fixed along the y direction, we indeed found the bond-centered hole stripes favored for $\alpha_x > \alpha_y$ (tilt axis along x , with the stripe perpendicular to it) and the site-centered hole stripes favored for $\alpha_x < \alpha_y$ (tilt axis along y , i.e., parallel to the stripes, similarly to what found for antiferromagnetic stripes in Ref.¹¹). The stability of the two possible stripe arrangements is evident in the inset of Figure 4, where ΔE , i.e., the energy of the stripe parallel to the tilt axis minus the energy of the stripe perpendicular to it, shows a different behavior for BC and SC stripes. Note that all data are in agreement with calculations using the Hellman-Feynman theorem (providing directly the slopes in the limit $\alpha_{x(y)} \rightarrow 1$), valid for small deformations, which gives $\Delta E/t = 0.00520\Delta t/t$ for bond-centered stripes and $\Delta E/t = -0.00167\Delta t/t$ for site-centered stripes. Remarkably, the RMFT approach also confirms that these superconducting modulated states are stabilized by tetragonal distortion (not shown). Instead, in the case of π -shift domain stripes, which involves higher energy scales, there is no appreciable difference in the behavior of the bond- and site-centered geometries with respect to the distortion axis, see Figure 5. Indeed, lattice deformation lowers the π DRVB energy in both cases with respect to the uniform RVB state, with a slightly more favorable contribution when the distortion axis lies on the y direction, i.e. parallel to the stripes.

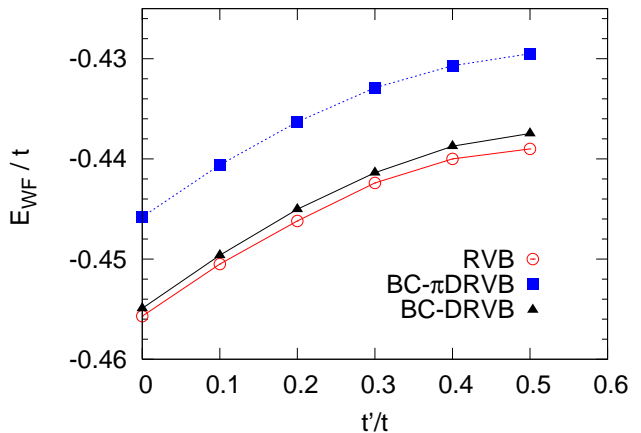


FIG. 6: (Color online) $t - t' - J$ model: Variational energy (in units of t) vs. t'/t for the uniform RVB (circles), the BC- π DRVB (squares) and the BC-DRVB (triangles) wavefunctions.

V. ROLE OF t'

Since the energies of the stripe states are very close to the homogeneous RVB state, some further contribution to the microscopic Hamiltonian could finally stabilize the bond-centered hole-stripe states as found in experiments. Here, we consider an additional hopping integral among next-nearest neighbor copper atoms, which is relevant, in many cuprates, for a correct description of their Fermi surface. The $t - t' - J$ Hamiltonian is obtained from the $t - J$ model of Eq. (1) by adding:

$$H_{t-t'-J} = H_{tJ} + t' \sum_{\langle\langle i,j \rangle\rangle \sigma} (c_{i\sigma}^\dagger c_{j\sigma} + h.c.) \quad (5)$$

where $\langle\langle i,j \rangle\rangle$ denotes next-nearest neighbors. Here, we take $t' > 0$ and $t/J = 3$, being relevant for hole-doped cuprates. In the presence of t' , a further variational hopping parameter χ'_{ij} among next-nearest neighbors is added to the mean-field Hamiltonian of Eq. (2). Considering the uniform RVB state, χ'_{ij} is homogeneous for all sites. Instead, in the case of stripe states, four different χ'_{ij} are optimized, according to the symmetries of the π DRVB and DRVB unitary cells. In Figure 6 we compare the variational energies of the two candidate stripe states, the π -phase domain RVB stripe and the inphase domain RVB stripe, with the energy of the homogeneous RVB state for different t' . It turns out that the DRVB stripe is the most stable inhomogeneous state, but, in both cases, the effect of t' is irrelevant for the stabilization of superconducting stripes.

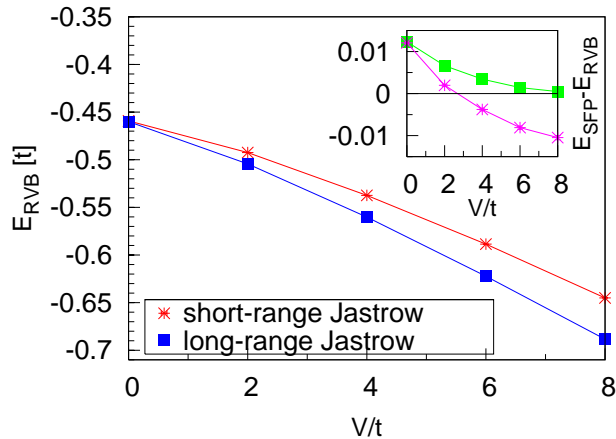


FIG. 7: (Color online) Energy of the homogeneous RVB state as a function of the Coulomb-repulsion strength V/t , in the presence of a short-range Jastrow factor (stars) and a long range Jastrow (squares). Inset: Energy difference between the SFP and the homogeneous RVB state as a function of the Coulomb-repulsion strength V/t . Both wavefunctions are optimized in the presence of a short-range (long-range) Jastrow factor, the energy difference being represented by stars (squares).

VI. ROLE OF NON-LOCAL COULOMB REPULSION

Finally, we consider the effect of a long-range Coulomb repulsion, which could play an important role in the STM measurements. To this purpose we consider the $t-J-V$ model:

$$H_{t-J-V} = H_{tJ} + \sum_{ij} V_{|i-j|} (n_i - \bar{n})(n_j - \bar{n}) \quad (6)$$

where \bar{n} is the average density of electrons. The potential $V_{|i-j|}$ has the form of a screened Coulomb repulsion $V_r = V \frac{\exp(-r/l_0)}{r}$, r being the periodized distance between different lattice sites. In the following, we have fixed $l_0 = 4$ and considered the properties of the system as a function of V . At the variational level, we find that, in the presence of a non-local Coulomb repulsion, a long-range Jastrow factor acting on the fully-projected mean-field state $|\Psi_G\rangle$ is needed:

$$|\Psi_J\rangle = \mathcal{P}_J |\Psi_G\rangle \quad (7)$$

where $\mathcal{P}_J = \exp\left[\frac{1}{2} \sum_{ij} v_{ij} n_i n_j\right]$, with $v_{ij} = v_{|i-j|}$ variational parameters which depend only on the distance $|i-j|$ and $|\Psi_G\rangle$ is defined in Eq. (3). This term takes into account the two-body correlations along all possible distances, and is necessary to get accurate wavefunctions in the presence of V_r . In Figure 7 we show the energy of the homogeneous RVB state, optimized with a short-range (i.e., up to nearest-neighbors) and a long-range Jastrow factor, respectively. It turns out that, by

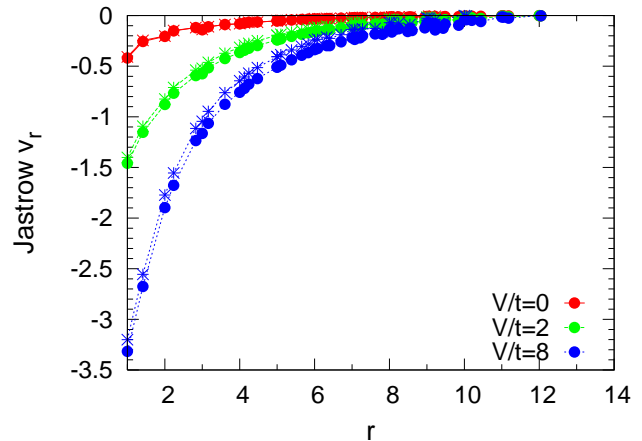


FIG. 8: (Color online) Jastrow parameter *vs.* distance for two tilted lattices on 242 (stars) and 338 sites (circles) and different values of V/t .

increasing V/t , the long-range correlation term plays a fundamental role in lowering the energy of the RVB variational state. Therefore, the addition of the long-range Jastrow term can strongly influence the hierarchy of variational phases stabilized at large V/t . Indeed, considering relative stability of the SFP with respect to the RVB state (see inset of Figure 7), it turns out that, with a short-range Jastrow, the SFP is the lowest-energy state already for $V \simeq 3t$, while the addition of a long-range Jastrow stabilizes the RVB state up to very large values of the Coulomb repulsion. To better understand the role played by the Jastrow factor in the presence of V_r , we optimize the RVB wavefunction for larger clusters. In Figure 8 we plot the resulting Jastrow parameters in real space. By increasing V , the correlation terms v_r increase, as expected. In particular, notice that the part at long distances is non-negligible even for $r > l_0$. Since a uniform Jastrow can promote the stability of uniform states and mask possible instabilities towards modulated states, we optimize the Jastrow parameters up to the next-nearest neighbor distance independently on the nonequivalent bonds (i.e. here the v_{ij} depend on i and j). The resulting energies are shown in Figure 9 where, even though the stripe energies approach the uniform RVB wavefunction by increasing V/t , the homogeneous state still remains the most stable. Notice that the presence of a long-range Jastrow factor stabilizes the BC- π DRVB state w.r.t. the SFP, at $V = 0$, contrarily to the values reported in Table I. However, by increasing V/t the SFP wavefunction gains energy and approaches closely the uniform RVB state. Moreover, considering the in-phase DRVB state, it turns out that for finite V/t the energy difference with respect to the RVB state is very small, of the order of the error bars. Unfortunately, in the presence of a non-local Coulomb repulsion, the main limit of this approach corresponds to the necessity of incorporating long-range Jastrow terms in order to reach

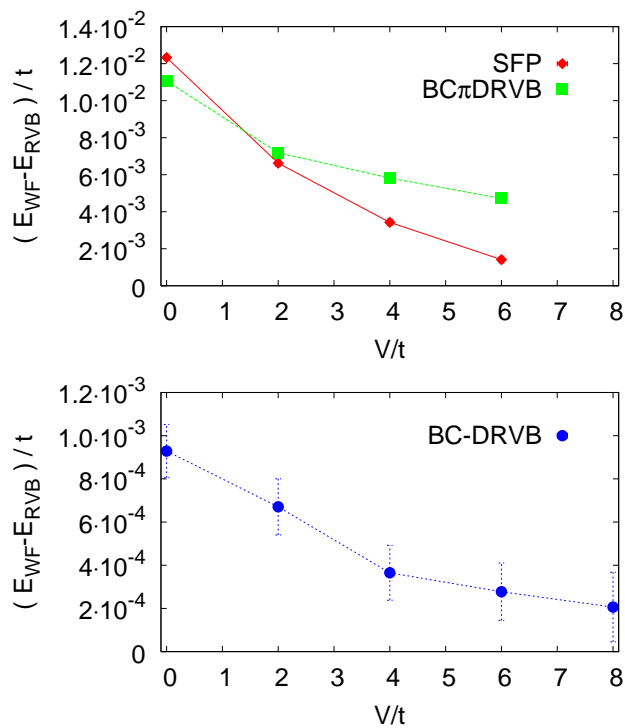


FIG. 9: (Color online) Energy difference w.r.t. the uniform RVB state of the SFP, π DRVB stripe state (top) and the DRVB state (bottom), as a function of V/t . All wavefunctions are optimized in the presence of a long-range Jastrow factor.

a good accuracy. Since the energies into play are very small, the restriction of homogeneous Jastrow terms at large distances, which governs the low-energy physics, could ultimately favor the uniform RVB state and bias our variational outcome. In other words, it might not be sufficient to assume inhomogeneous Jastrow terms at short distances. However, these variational results sug-

gest already that long-range Coulomb repulsion can be a driving force for the stabilization of modulated states.

VII. SUMMARY AND CONCLUSIONS

In summary, we have shown that unidirectionally modulated superconducting states are remarkably close in energy to the uniform RVB state. This is the case both for π -phase shift domain RVB stripes and for inphase domain RVB stripes. Their properties reflect the recent STM observations, both concerning the modulated charge and superconducting features. Besides the lattice distortion, long-ranged Coulomb repulsion further stabilizes the non-uniform superconducting stripe phases. Instead, next-nearest neighbor hopping does not seem to play any role in the hierarchy of phases studied here. However, although the stripe energies can approach very closely that of the homogeneous RVB state, so far the uniform solution remains the most stable. In particular, we have found that a π -phase shift costs more energy than the inphase counterpart having simple $\Delta = 0$ domains. Experiments suggest that the real stabilization of hole-stripes might imply some further factors than those investigated here.

Besides the perturbations to the $t - J$ Hamiltonian considered in this paper, it would be interesting to study the effect of disorder in HTSC materials which, according to recent calculations²⁸, could be relevant in stabilizing this kind of superstructures.

We thank F. Becca and S. Sorella for important discussions. M. C. and D. P. acknowledge the Agence Nationale de la Recherche (France) for support. M. R. thanks the Foundation for Polish Science (FNP) and the Polish Ministry of Science and Education under Project No. N202 068 32/1481 for support.

¹ K. Tanaka, W. S. Lee, D. H. Lu, A. Fujimori, T. Fujii, Risdiana, I. Terasaki, D. J. Scalapino, T. P. Devereaux, Z. Hussain, and Z.-X. Shen, *Science* **314**, 1910 (2006).
² K. M. Shen, F. Ronning, D. H. Lu, F. Baumberger, N. J. C. Ingle, W. S. Lee, W. Meevasana, Y. Kohsaka, M. Azuma, M. Takano, H. Takagi, and Z.-X. Shen, *Science* **307**, 901 (2005).
³ J. M. Tranquada, B. J. Sternlieb, J. D. Axe, Y. Nakamura, and S. Uchida, *Nature* **375**, 561 (1995).
⁴ J. A. Robertson, S. A. Kivelson, E. Fradkin, A. C. Fang, and A. Kapitulnik, *Phys. Rev. B* **74**, 134507 (2006).
⁵ Y. Kohsaka, C. Taylor, K. Fujita, A. Schmidt, C. Lupien, T. Hanaguri, M. Azuma, M. Takano, H. Eisaki, H. Takagi, S. Uchida, and J. C. Davis, *Science* **315**, 1380 (2007).
⁶ J. Zaanen and O. Gunnarsson, *Phys. Rev. B* **40**, 7391 (1989); K. Machida, *Physica C* **158**, 192 (1989); D. Poilblanc, and T. M. Rice, *ibid.* **39**, 9749 (1989).
⁷ D. LeBoeuf, N. Doiron-Leyraud, J. Levallois, R. Daou, J.-

B. Bonnemaïson, N. E. Hussey, L. Balicas, B. J. Ramshaw, R. Liang, D. A. Bonn, W. N. Hardy, S. Adachi, C. Proust, and L. Taillefer, *Nature* **450**, 533 (2007).
⁸ A. Himeda, T. Kato, M. Ogata, *Phys. Rev. Lett.* **88**, 117001 (2002).
⁹ C. Weber, D. Poilblanc, S. Capponi, F. Mila, and C. Jaudet, *Phys. Rev. B* **74**, 104506 (2006).
¹⁰ B. Büchner, M. Breuer, A. Freimuth, and A. P. Kampf, *Phys. Rev. Lett.* **73**, 1841 (1994).
¹¹ A. P. Kampf, D. J. Scalapino, and S. R. White, *Phys. Rev. B* **64**, 052509 (2001).
¹² F. Becca, L. Capriotti, and S. Sorella, *Phys. Rev. Lett.* **87**, 167005 (2001).
¹³ F. C. Zhang and T. M. Rice *Phys. Rev. B* **37**, 3759 (1988).
¹⁴ P. W. Anderson, *Science* **235**, 1196 (1987).
¹⁵ S. Sorella, G. B. Martins, F. Becca, C. Gazza, L. Capriotti, A. Parola, and E. Dagotto, *Phys. Rev. Lett.* **88**, 117002 (2002).

- ¹⁶ L. Spanu, M. Lugas, F. Becca, and S. Sorella, Phys. Rev. B **77**, 024510 (2008).
- ¹⁷ F. C. Zhang, C. Gros, T. M. Rice, and H. Shiba, Supercond. Sci. Technol. **1**, 36 (1988).
- ¹⁸ M. Raczkowski, D. Poilblanc, R. Frésard, and A. M. Oleś, Phys. Rev. B **75**, 094505 (2007).
- ¹⁹ M. Raczkowski, M. Capello, and D. Poilblanc, submitted to Acta Phys. Pol. A.
- ²⁰ S. Sorella, Phys. Rev. B **64**, 024512 (2001).
- ²¹ I. Affleck and J. B. Marston, Phys. Rev. B **37**, R3774 (1988).
- ²² M. Raczkowski, M. Capello, D. Poilblanc, R. Frésard, and A. M. Oleś, Phys. Rev. B **76**, 140505(R) (2007).
- ²³ Q. Li, M. Hücker, G. D. Gu, A. M. Tsvelik, and J. M. Tranquada, Phys. Rev. Lett. **99**, 067001 (2007).
- ²⁴ E. Berg, E. Fradkin, E.-A. Kim, S. A. Kivelson, V. Oganesyan, J. M. Tranquada, and S. C. Zhang, Phys. Rev. Lett. **99**, 127003 (2007); see also Ref.⁸.
- ²⁵ M. Vojta and O. Rösch, Phys. Rev. B **77**, 094504 (2008); S. Baruch and D. Orgad, Phys. Rev. B **77**, 174502 (2008).
- ²⁶ Indeed, considering that decreasing J along one direction leads to smaller Δ_{ij} for the bonds in that direction, whereas decreasing t produces the opposite, we deduce that the kinetic contribution dominates this competition (the same effect occurs also in the RVB state with rotational symmetry breaking).
- ²⁷ In presence of lattice distortion, different vertical and horizontal bonds are assumed for the reference homogeneous RVB state.
- ²⁸ M. A. Metlitski and S. Sachdev, Phys. Rev. B **77**, 054411 (2008).